© 2021. Published by The Company of Biologists Ltd | Development (2021) 148, dev195057. doi:10.1242/dev.195057

STEM CELLS AND REGENERATION

RESEARCH ARTICLE

Ecdysone regulates the *Drosophila* imaginal disc epithelial barrier, determining the length of regeneration checkpoint delay

Danielle DaCrema, Rajan Bhandari, Faith Karanja, Ryunosuke Yano and Adrian Halme*

ABSTRACT

Regeneration of *Drosophila* imaginal discs, larval precursors to adult tissues, activates a regeneration checkpoint that coordinates regenerative growth with developmental progression. This regeneration checkpoint results from the release of the relaxin-family peptide Dilp8 from regenerating imaginal tissues. Secreted Dilp8 protein is detected within the imaginal disc lumen, in which it is separated from its receptor target Lgr3, which is expressed in the brain and prothoracic gland, by the disc epithelial barrier. Here, we demonstrate that following damage the imaginal disc epithelial barrier limits Dilp8 signaling and the duration of regeneration checkpoint delay. We also find that the barrier becomes increasingly impermeable to the transepithelial diffusion of labeled dextran during the second half of the third instar. This change in barrier permeability is driven by the steroid hormone ecdysone and correlates with changes in localization of Coracle, a component of the septate junctions that is required for the late-larval impermeable epithelial barrier. Based on these observations, we propose that the imaginal disc epithelial barrier regulates the duration of the regenerative checkpoint, providing a mechanism by which tissue function can signal the completion of regeneration.

KEY WORDS: Epithelial barrier, Septate junction, Regeneration, Dilp8, Ecdysone, *Drosophila*

INTRODUCTION

Drosophila melanogaster imaginal discs, larval precursors to adult organs, can regenerate early in development, but they lose this regenerative ability before pupating (Halme et al., 2010). Regeneration activates a developmental checkpoint (regeneration checkpoint) through release of the relaxin peptide *Drosophila* insulin-like peptide 8 (Dilp8; also known as Ilp8) (Colombani et al., 2012; Garelli et al., 2012). Dilp8 functions in the brain and the prothoracic gland (PG) by binding the relaxin receptor Lgr3, which inhibits the synthesis of the steroid hormone ecdysone (Colombani et al., 2015; Garelli et al., 2015; Jaszczak et al., 2016; Vallejo et al., 2015). As ecdysone triggers both pupariation and limits regeneration (Hackney and Cherbas, 2014; Halme et al., 2010), the inhibition of ecdysone synthesis during the regeneration checkpoint extends the larval phase, coordinating regeneration with developmental progression (Halme et al., 2010; Jaszczak et al., 2016). It remains unclear what events signal the completion of regeneration and determine the duration of the regenerative checkpoint delay, allowing larvae to pupate and progress through development.

Dilp8 has been observed in the lumen of wing imaginal discs, between the primary and peripodial epithelia (Colombani et al., 2012). As imaginal discs derive from the larval epidermis, and emerge into the body cavity, the disc lumen is topologically separated from the hemolymph by the imaginal disc epithelia (Pastor-Pareja et al., 2004). This led us to hypothesize that the imaginal disc epithelial barrier (EB) might regulate Dilp8 signaling by holding Dilp8 in the disc lumen, blocking Dilp8-Lgr3 signaling in the brain and PG.

The EB is a semi-permeable diffusion barrier between adjacent epithelial cells formed by tight junctions in vertebrates and septate junctions (SJs) in invertebrates (Tepass et al., 2001). Claudin proteins determine EB exclusivity likely by homo- and heterodimerizing with the claudins of neighboring cells to form size- and charge-selective pores (Furuse and Tsukita, 2006; Suzuki et al., 2015). Claudins are localized to and stabilized at SJs by a large core complex (Izumi and Furuse, 2014). Although the assembly and function of each member of the SJs is not well understood, one known subcomplex includes Coracle (Cora), a member of the Protein 4.1 superfamily (Fehon et al., 1994), and Neurexin-IV (Nrx; also known as Nrx-IV) (Baumgartner et al., 1996). *In vivo*, Cora and Nrx localize to the SJs and are necessary for stabilizing claudins at the SJs and for barrier activity (Baumgartner et al., 1996; Fehon et al., 1994; Genova and Fehon, 2003).

Here, we demonstrate that the EB of wing imaginal discs matures during the third instar in response to increasing ecdysone levels and a re-localization of Cora along the lateral membrane. This mature, prepupal EB limits Dilp8 signaling and determines the duration of the developmental checkpoint after damage.

RESULTS

The activity of Dilp8 is constrained by the imaginal disc epithelial barrier, determining the duration of regeneration checkpoint delay

Previously, Colombani et al. detected Dilp8 in the lumen between the primary wing disc epithelium and the peripodial epithelium, a region topologically separate from the larval hemolymph (Colombani et al., 2012; Pastor-Pareja et al., 2004). We recapitulated these findings by exogenously expressing a FLAG epitope-tagged allele of Dilp8 (Dilp8::FLAG; Garelli et al., 2012) in wing imaginal discs with *apterous-Gal4* (*Ap-Gal4*) to induce expression in the dorsal half of the tissue (Cohen et al., 1992). We also detected an accumulation of Dilp8::FLAG in the imaginal disc lumen (Fig. 1A-D; Fig. S1A-C). This observation led us to hypothesize that luminal localization might limit Dilp8 signaling by preventing access to the brain and PG, in which the Dilp8 receptor Lgr3 regulates growth and developmental timing (Colombani et al., 2015; Garelli et al., 2015; Vallejo et al., 2015). To test this, we first investigated whether the accumulation of Dilp8::FLAG in the wing disc lumen is dependent on the EB in the

Department of Cell Biology, University of Virginia School of Medicine, Charlottesville, VA 22902, USA.

*Author for correspondence (ajh6a@virginia.edu)

A.H., 0000-0002-6608-5305

Handling Editor: Kenneth Poss
Received 16 July 2020; Accepted 15 February 2021

Development (2021) 148, dev195057. doi:10.1242/dev.195057

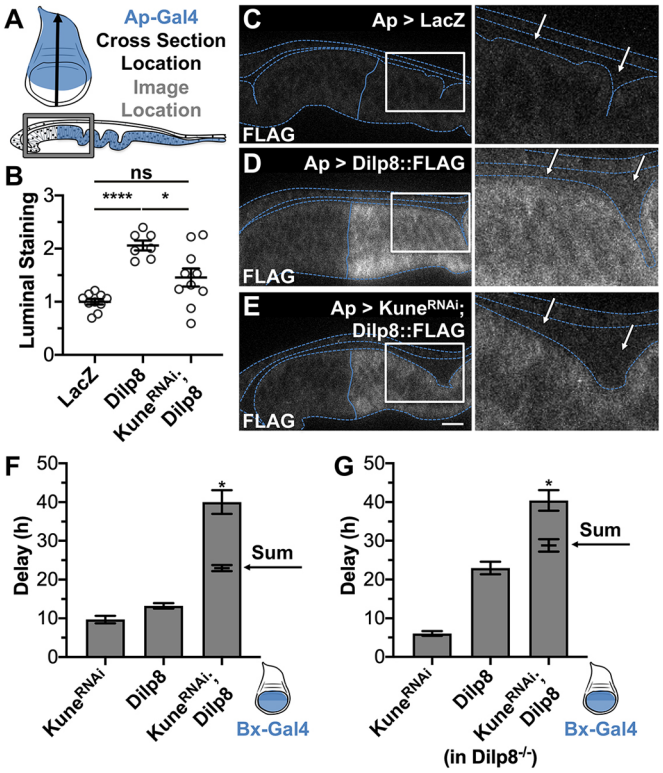

Fig. 1. The epithelial barrier limits Dilp8 signaling. (A) *Ap-Gal4* expresses in the dorsal half of wing imaginal discs. Blue indicates the expression region along the *xy* plane (top) and *xz* plane (bottom, cross section of top image; arrowhead in top image corresponds with right hand side of bottom image). Confocal *xz* images were collected from the pouch region (gray box). (B-E) Dilp8::FLAG is contained in the imaginal disc lumen by the SJ component, Kune. (B) Quantification of FLAG fluorescence in the lumen of wing imaginal discs expressing control (*Ap>lacZ*), Dilp8::FLAG alone (*Ap>dilp8::FLAG*), or co-expressing *kune*^{RNAi} and Dilp8::FLAG (*Ap>kune*^{RNAi}*;dilp8*). Normalized to *lacZ*. (C-E) Representative images of the quantification in B. Dashed blue line indicates tissue outline defined by Actin (Rhodamine Phalloidin, Fig. S1A-C). Solid blue line indicates dorsal-ventral boundary defined by *lacZ* co-expression (controls contain two copies of *UAS-lacZ*), (anti-βGal, Fig. S1A-C). White box indicates magnified regions shown in right-hand panels. White arrows indicate the lumen. (F,G) Co-expression of *kune*^{RNAi} and Dilp8 induces synergistic delay in a wild-type background (F) or when endogenous Dilp8 is limited by expression in a Dilp8 mutant background (Dilp8^{MI00727}/Dilp8^{MI00727}; Garelli et al., 2012) (G). Ectopic expression by *Bx-Gal4* (blue indicates expression area) of *kune*^{RNAi}, Dilp8, or co-expression of *kune*^{RNAi} and Dilp8 (*kune*^{RNAi}; Dilp8) induces developmental delay compared with *lacZ*-expressing controls (median pupariation times, Fig. S1B). Arrows indicate the sum value of the delay induced by *kune*^{RNAi} and Dilp8 expressed alone. Data are mean±s.e.m. In B, individual points represent single images collected from two independent experiments. *lacZ*, *n*=10; Dilp8, *n*=7: *kune*^{RNAi}; Dilp8, *n*=10 discs. In F,G, data were collected from at least three independent experiments. ns, not significant. **P*<0.05, *****P*<0.0001 calculated by Brown-Forsythe and Welch ANOVA with Dunnett's T3 multiple comparison test (B), or from one sample *t*-test comparing the additive value and observed delay (F,G). Scale bar: 10 µm.

primary wing disc epithelium. To disrupt the EB, we expressed the Dilp8::FLAG construct along with an RNAi construct targeting the claudin Kune-Kune (Kune; see Fig. S1D for *kune*^{RNAi} knockdown efficiency), a necessary component of the imaginal disc EB (Nelson et al., 2010). When the EB is disrupted, we see significantly less Dilp8::FLAG accumulate in the lumen of the wing disc (Fig. 1B,E), demonstrating that the EB of the primary wing disc epithelium retains Dilp8::FLAG in the imaginal disc lumen.

We then examined whether disruption of the EB produces increased developmental checkpoint signaling following Dilp8 expression in the wing disc. To test this, we used *beadex-Gal4* (*Bx-Gal4*) to express either *dilp8::FLAG* alone, *kune*^{RNAi} alone, or both constructs together in the pouch region of the wing disc (Milán et al., 1998) and measured regeneration checkpoint delay relative to *lacZ*-expressing control larvae (Fig. 1F; Fig. S2A). Dilp8::FLAG and *kune*^{RNAi} each produced slightly delayed larvae relative to controls (13 and 10 hours delay, respectively), whereas the co-expression of Dilp8 and *kune*^{RNAi} produced a strong genetic interaction and a synergistic delay (40 hours delay; Fig. 1F). These results are consistent with our observation that Kune is required for luminal Dilp8 accumulation in the wing disc (Fig. 1C-E).

We were concerned that the synergistic delay we observed during Dilp8 and *kune*^{RNAi} co-expression might reflect, in part, the effect of *kune*^{RNAi} on endogenous *dilp8*. In particular, loss of SJ components have been shown to downregulate the Hippo pathway, which could lead to transcriptional activation of the endogenous copies of *dilp8* (Khadilkar and Tanentzapf, 2019; Lee et al., 2020). To confirm that the synergistic effect on delay is not due to increased endogenous *dilp8* activity, we examined the effect of co-expression of Dilp8 and *kune*^{RNAi} in a homozygous *dilp8* mutant background. Even without functional endogenous *dilp8*, we still observed a genetic interaction between Dilp8::FLAG and *kune*^{RNAi} and a synergistic delay (Fig. 1G). Therefore, we conclude that *kune*^{RNAi} genetically interacts with the UAS-regulated transgenic Dilp8 in these experiments, which is unlikely to be affected by changes in Hippo signaling. We generated similar synergistic interactions when we co-expressed Dilp8::FLAG and *nrx*^{RNAi} (Fig. S2C-F). Although these data do not exclude the possibility that some Dilp8 is released through the basal or basal-lateral surfaces of cells, these results demonstrate that the EB limits Dilp8 signaling from the wing imaginal disc by retaining Dilp8 in the wing disc lumen.

The wing imaginal disc epithelial barrier becomes more impermeable during the last larval instar

The experiments above demonstrate that the wing disc EB can limit Dilp8 signaling. However, Dilp8 expression in the wing disc produces developmental delay even without EB disruption in the wing (Fig. 1F,G; Colombani et al., 2012; Garelli et al., 2012). In addition, basal levels of Dilp8 in the developing wing disc regulate tissue symmetry through Lgr3 in the brain (Colombani et al., 2012; Garelli et al., 2012, 2015; Vallejo et al., 2015). To reconcile these observations with the sequestration of Dilp8 in the wing disc lumen in late third instar larvae, we hypothesized that there may be changes in EB permeability during development. To examine this, we developed a quantitative method for measuring EB permeability that is an extension of that described in Lamb et al. (1998), which used the ability of fluorophore-conjugated dextran to enter the lumen of a tissue to assess EB function (Lamb et al., 1998). We incubated inverted larval carcasses in solution containing fluorescein-conjugated dextran for 30 min before paraformaldehyde fixation. We mounted and imaged the fixed imaginal discs, then measured the fluorescein signal in the lumen of the imaginal discs to quantify EB permeability (see Materials and Methods and Fig. S3).

When we examined late third instar imaginal discs (116 h after egg deposition; h AED), we detected very little fluorescent signal in the wing disc lumen (Fig. 2A; Fig. S3A,B). To determine whether exclusion of dextran from late larval wing discs is dependent on EB function, we measured fluorescence in imaginal discs that were punctured with forceps before dextran incubation. As expected, we observed that puncturing the wing disc caused a substantial increase in luminal fluorescence in these discs (Fig. 2A; Fig. S3C), demonstrating that an intact epithelium is necessary for the

Development (2021) 148, dev195057. doi:10.1242/dev.195057

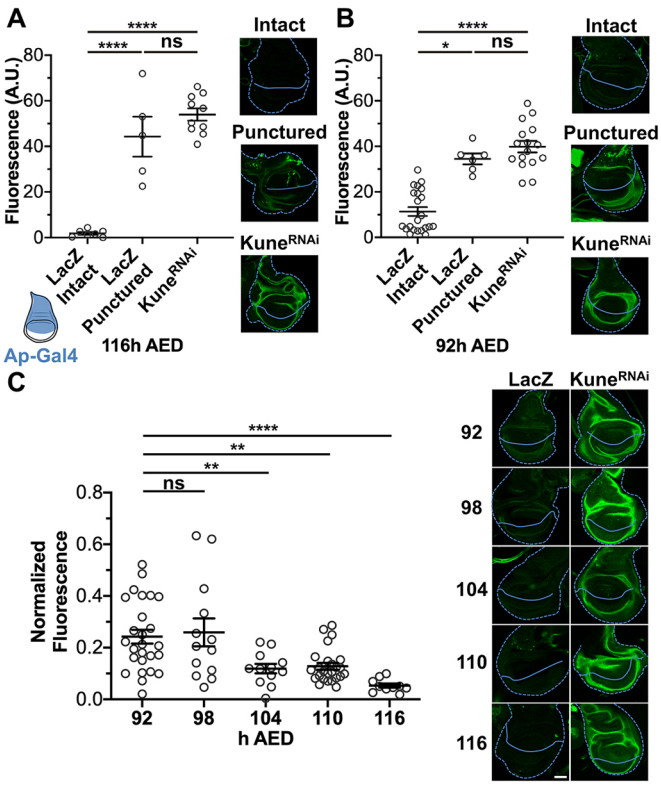

Fig. 2. The wing disc epithelial barrier becomes more impermeable with progression through the third larval instar. (A,B) The wing imaginal disc EB excludes 10 kD dextran and the function of the barrier is dependent on Kune at both 116 h (A) and 92 h AED (B). *lacZ* and *kune*^{RNAi} were expressed with *Ap-Gal4* (blue indicates expression area). Luminal intensity was measured in *lacZ* controls, *lacZ* controls that were punctured during dissection before fixing, and *kune*^{RNAi}-expressing discs. Representative dextran images for each condition are on the right. Dotted blue lines indicate tissue outline defined by Actin (Rhodamine Phalloidin); solid blue line indicates dorsal ventral boundary defined by *lacZ* (anti-βGal). (C) The EB gradually becomes less permeable between 92 h and 116 h AED. Barrier function was measured every 6 h from 92 h to 116 h AED in *Ap>lacZ* or *Ap>kune*^{RNAi} wing imaginal discs and normalized to the mean luminal intensity of the *kune*^{RNAi}-expressing discs at each timepoint (*kune*^{RNAi} data represented in Fig. S6). Panels on the right show representative dextran images for each condition. Dashed blue line indicates tissue outline defined by Actin (Rhodamine Phalloidin). Solid blue line indicates dorsal ventral boundary defined by *lacZ* (anti-βGal). Data are mean±s.e.m.; individual points represent single images. Left to right: *n*=7, 5, 10 (A); *n*=22, 6, 16 (B); *n*=26, 13, 12, 25, 10 (C). ns, not significant. **P*<0.05, ***P*<0.01, *****P*<0.0001 calculated by Brown-Forsythe and Welch ANOVA with Dunnett's T3 test for multiple comparisons (A,C) or one-way ANOVA with Tukey test for multiple comparisons (B). Scale bar: 50 µm.

exclusion of dextran from the lumen of late third instar wing discs. We then tested whether this exclusion reflected the activity of the EB by measuring dextran infiltration into wing discs expressing *kune*^{RNAi} (*Ap>kune*^{RNAi}). Consistent with a crucial role of Kune in wing EB function, we observed an equivalent amount of luminal fluorescence in *Ap>kune*^{RNAi} discs as in punctured discs (Fig. 2A). However, we also observed that expression of *kune*^{RNAi} in the wing disc produced a modest increase in cell death within the disc (Fig. S4). Although we cannot exclude the possibility that apoptosis induced by *kune*^{RNAi} expression contributes to barrier disruption, our data demonstrate that loss of *kune* completely disrupts the EB in late third instar wing discs.

To characterize the EB in younger wing discs, we examined wing discs 24 h earlier in development (92 h AED, the middle of the third instar) when disc damage and/or Dilp8 expression still produces developmental delay. Similar to our observations at 116 h AED, in 92 h AED discs we observed that physical puncture and *kune*^{RNAi} expression both increased dextran infiltration into the wing disc lumen (Fig. 2B). This indicates that wing imaginal discs in the middle of the third instar have a functioning EB, mediated by *kune*, which limits the diffusion of dextran across the epithelium. We also noticed that the level of dextran infiltration into control 92 h AED wing discs appeared to be much higher than the fluorescence observed at 116 h AED (compare Fig. 2A and B; Fig. S3A), suggesting that the EB of the wing disc grows more impermeable towards the end of the third instar. We also observed this change in barrier permeability from 92 h to 116 h AED with 70 kD dextran (Fig. S5), suggesting that the permeability change does not reflect a change in size selectivity.

To further characterize the maturation of the more impermeable barrier, we used our quantitative permeability assay to examine dextran infiltration at 6 h intervals between 92 h and 116 h AED. We normalized the fluorescence intensity to discs of equivalently staged larvae with barriers disrupted by *kune*^{RNAi} expression. Consistent with our earlier observations, as the wing disc develops, we see a progressive decrease in dextran in the wing disc lumen, suggesting a decrease in EB permeability (Fig. 2C; for individual fluorescence distributions and independent replicates see Fig. S6A-C). This change in barrier permeability is not accompanied by loss of proliferative activity in the wing disc, as we still see mitotic cells within 116 h AED discs (Fig. S6D-F), demonstrating that the loss of barrier permeability precedes the completion of disc growth.

Based on these observations, we conclude that the wing disc EB limits diffusion throughout the third instar, as we see an increase in permeability in punctured or *kune*^{RNAi} expressing discs at all timepoints. However, we see a substantial decrease in permeability of the barrier as larvae advance through the third instar.

Changes in epithelial barrier permeability correlate with changes in junctional protein expression and localization

The changes in barrier permeability during the last larval instar could be attributable to changes in localization and/or activity of different components of the EB. To address this, we examined the localization Kune, Cora and Nrx. Using indirect immunofluorescent staining with a Kune-directed antibody (Nelson et al., 2010), we observed that Kune localized to the apical-lateral membrane throughout the third instar at which SJs localize (Fig. 3A,B; Fig. S7A,B) (Lamb et al., 1998; Ward IV et al., 2001). However, the amount of Kune signal at the SJs increased during the late third instar (Fig. 3C; quantification described in Materials and Methods and Fig. S8). To localize Nrx, we used a functional Nrx-GFP fusion (Buszczak et al., 2007; Morin et al., 2001). Like Kune, Nrx-GFP localized to the SJs throughout the third instar and increased in signal intensity from 92 h to 116 h AED (Fig. 3D-F; Fig. S7D,E). In contrast to Kune and Nrx-GFP, Cora localization was more dynamic. Using indirect immunofluorescence staining with a Cora-targeted antibody (C615.16; Developmental Studies Hybridoma Bank), we saw that at 92 h AED Cora was localized either with slight or no selectivity for the SJs (Fig. 3G,I; Fig. S7F). However, by 116 h AED, Cora localization was restricted to the apical-lateral localization at the SJs, similar to Kune and Nrx-GFP (Fig. 3H,I; Fig. S7G).

In summary, we observed an increase in Kune and Nrx localization at the SJ, and a refinement of Cora localization, from a broader distribution along the lateral membrane to localization at the apical-lateral site of the SJs. These changes in SJ component localization correlate with the maturation of the disc EB.

Development (2021) 148, dev195057. doi:10.1242/dev.195057

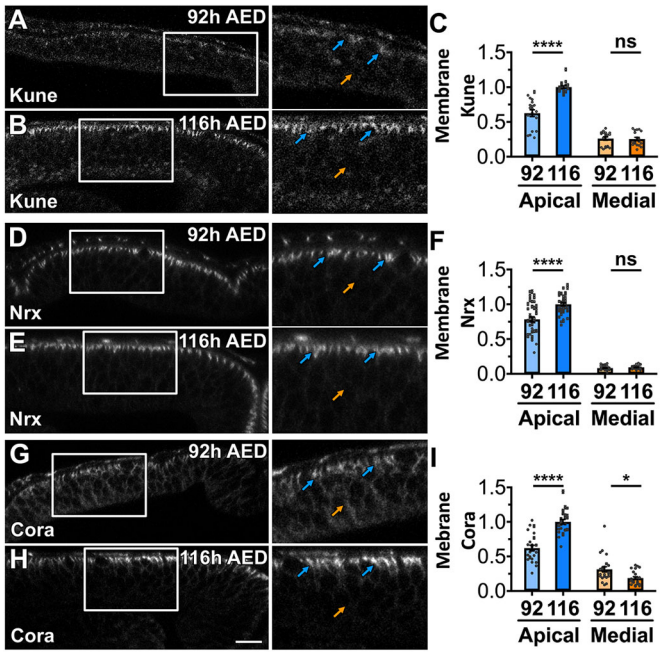

Fig. 3. The localization of septate junction components changes between 92 h and 116 h AED. (A-C) Representative images of Kune localization at 92 h (A) and 116 h AED (B) showing apical-lateral localization. (C) Quantification of Kune localized along the apical-lateral and medial-lateral membrane. (D-F) Representative images of Nrx localization at 92 h (D) and 116 h AED (E) showing apical-lateral localization. (F) Quantification of Nrx localized along the apical-lateral and medial-lateral membrane. (G-I) Representative images of Cora localization at 92 h (G) and 116 h AED (H) showing diffuse Cora localization at 92 h AED and apical-lateral Cora localization at 116 h AED. (I) Quantification of Cora localized along the apical-lateral and medial-lateral membrane. (C,F,I) Individual points represent mean±s.e.m. for each image, with *n* as the number of cell-cell interactions across the region. Bars represent mean±s.e.m. across the images, with *n* as the number of images. Data normalized to the apical-lateral localization of each component at 116 h AED. The quantification method is explained in Materials and Methods and Fig. S8. Images are representative cross-sections of the pouch region of the wing imaginal discs collected by capturing *xz* images. All images are oriented dorsal to the right. White boxes indicate magnified region shown on right, blue arrows indicate apical-lateral localization, orange arrows indicate medial-lateral localization (or lack thereof). Actin localization in Fig. S7. *n*=19 (A,C), 18 (B,C), 39 (D,F), 41 (E,F), 24 (G,I) and 24 (H,I) images. ns, not significant. **P*<0.05, *****P*<0.0001 calculated by Brown-Forsythe and Welch ANOVA with Dunnett's T3 test for multiple comparisons. Scale bar: 10 µm.

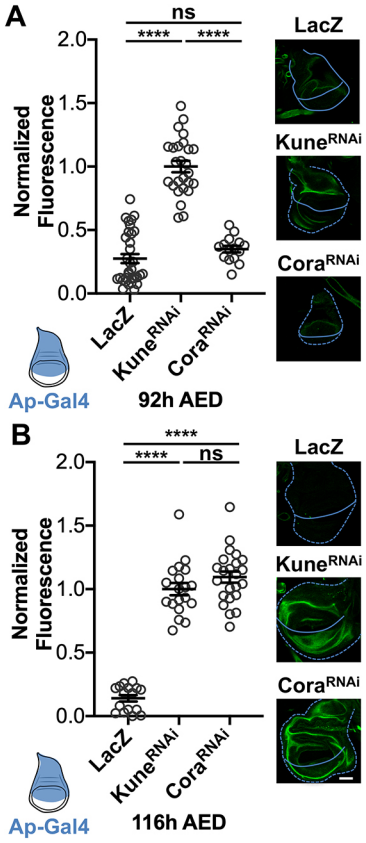

Fig. 4. The requirement for Cora in epithelial barrier activity changes between 92 h and 116 h AED. (A,B) Function of the EB in discs expressing *Ap>lacZ*, *Ap>kune*^{RNAi} or *Ap>cora*^{RNAi} (blue indicates expression area) to exclude 10 kD dextran at 92 h (A) and 116 h AED (B). Representative images of 10 kD dextran for each condition on the right. Dashed blue line indicates tissue outline defined by Actin (Rhodamine Phalloidin). Solid blue line indicates dorsal-ventral boundary defined by *lacZ* (anti-βGal). At 92 h AED the barrier permeability of *cora*^{RNAi}-expressing discs is similar to that of *lacZ*-expressing discs. At 116 h AED, the barrier permeability of *cora*^{RNAi}-expressing discs is similar to *kune*^{RNAi}-expressing discs. Normalized to mean luminal intensity of *kune*^{RNAi}-expressing discs. Data are mean±s.e.m.; individual points represent single images. Left to right: *n*=33, 26, 15 images (A); *n*=16, 19, 23 images (B). ns, not significant. *****P*<0.0001 calculated by Brown-Forsythe and Welch ANOVA with Dunnett's T3 test for multiple comparisons. Scale bar: 50 µm.

Coracle is required to produce the changes in epithelial barrier permeability during the last larval instar

To determine whether Cora activity is important for the decrease in EB permeability during the last larval instar, we examined the effect of *cora*^{RNAi} expression on wing disc barrier permeability. At 92 h AED, *Ap>cora*^{RNAi} did not impact wing EB permeability. The barrier activity in Cora knockdown discs is similar to control (*Ap>lacZ*) discs, with greater selectivity than *Ap>kune*^{RNAi}-expressing discs, which have no functioning barrier (Fig. 4A). In contrast, by 116 h AED *Ap>cora*^{RNAi}-expressing discs exhibited a completely disrupted EB, comparable with *Ap>kune*^{RNAi}-expressing discs (Fig. 4B). Therefore, as the third instar progresses, there is a change in the role of Cora for EB activity: 92 h AED wing discs had a weaker, somewhat permeable, barrier that requires Kune, but not Cora, whereas 116 h AED wing discs had a more impermeable barrier dependent on both Kune and Cora.

Cora, Kune and Nrx localize interdependently at the SJs during the development of the embryonic tracheal epithelia (Nelson et al., 2010; Oshima and Fehon, 2011). We examined whether the same interdependence occurs in the wing imaginal disc and whether it changes during development. To do this, we visualized the localization of Cora, Kune, and Nrx-GFP in discs expressing an *Ap-Gal4*-driven RNAi construct targeted against one of these components. Predictably, expression of the RNAi's targeting Cora, Kune, and Nrx significantly reduced protein expression of the targeted gene in the dorsal compartment of both 92 h and 116 h AED wing discs (Figs. S9-S11B,C), demonstrating the efficacy of the RNAi constructs. We then examined the interdependence for localization of these three SJ proteins at 92 h and 116 h AED wing discs (Fig. 5A-F; quantified in Figs. S9-S11D-I). Nrx localization at the SJs in 92 h AED discs depended on both Kune (*Ap>kune*^{RNAi}; Fig. 5A; Fig. S9E) and Cora (*Ap>cora*^{RNAi}; Fig. 5E; Fig. S11E). At 116 h AED, Nrx localization at the SJ was also dependent on both Kune and Cora (Fig. 5B,F; Figs S9H, S11H). Likewise, the SJ localization of Kune at both 92 h and 116 h AED was dependent on Nrx (*Ap>nrx*^{RNAi}; Fig. 5C,D; Fig. S10D,G) and, surprisingly, Cora (*Ap>cora*^{RNAi}; Fig. 5E,F; Fig. S11D,G). At 92 h AED, the

Development (2021) 148, dev195057. doi:10.1242/dev.195057

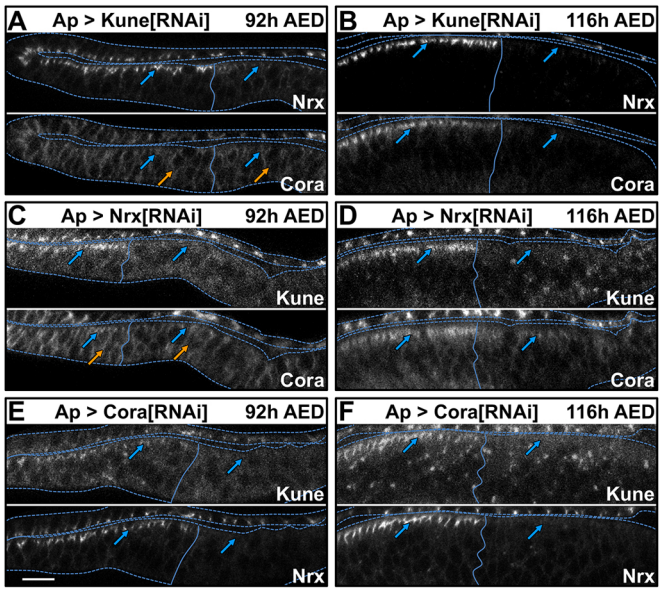

Fig. 5. The localization of Nrx and Kune is dependent on Cora at both 92 h and 116 h AED. (A-F) *Ap-Gal4* was used to express $kune^{RNAi}$, nrx^{RNAi} or $cora^{RNAi}$ and the localization of Kune, Nrx and Cora was assessed. Images span the dorsal-ventral boundary (solid line, defined by RNAi knockdown of the targeted protein; Figs S9-S11); the dorsal region (Gal4 expression area) is on the right. Dashed lines represent tissue outline defined by Actin staining (Fig. S8). Blue arrows indicate apical-lateral localization, orange arrows indicate medial-lateral localization. (A,B) Localization of Nrx (top) and Cora (bottom) in *Ap>*$kune^{RNAi}$-expressing discs at 92 h (A) and 116 h AED (B). In the portion of the disc without $kune^{RNAi}$ expression Nrx is apical-laterally localized at 92 h and 116 h AED. Nrx intensity localization is lost with $kune^{RNAi}$ expression at both times. Cora localization is independent of Kune at 92 h AED, but is significantly depleted with $kune^{RNAi}$ expression at 116 h AED. Kune localization in *Ap>*$kune^{RNAi}$-expressing discs and the localization quantifications for each component are in Fig. S9. (C,D) Localization of Kune (top) and Cora (bottom) in *Ap>*nrx^{RNAi}-expressing discs at 92 h (C) and 116 h AED (D). Kune localization is lost with nrx^{RNAi} expression at both times. At 92 h AED, Cora localization is only slightly dependent on Nrx, but is significantly depleted with nrx^{RNAi} expression at 116 h AED. Nrx localization in *Ap>*nrx^{RNAi}-expressing discs and the localization quantifications for each component are in Fig. S10. (E,F) Localization of Kune (top) and Nrx (bottom) in *Ap>*$cora^{RNAi}$-expressing discs at 92 h (E) and 116 h AED (F). Kune and Nrx localization are significantly depleted with $cora^{RNAi}$ at both times. Cora localization in *Ap>*$cora^{RNAi}$-expressing discs and the localization quantifications for each component are in Fig. S11. Images are representative from *n*=5 (A), 9 (B), 8 (C), 11 (D), 6 (E), 11 (F) images. Scale bar: 10 µm.

localization of Cora along the lateral membrane was unaffected by RNAi-targeted knockdown of either Kune (*Ap>*$kune^{RNAi}$; Fig. 5A; Fig. S9F) or Nrx (*Ap>*nrx^{RNAi}; Fig. 5C; Fig. S10F). However, the localization of Cora at the SJs at 116 h AED was disrupted by RNAi-targeted knockdown of either Kune (*Ap>*$kune^{RNAi}$; Fig. 5B; Fig. S9G) or Nrx (*Ap>*nrx^{RNAi}; Fig. 5D; Fig. S10G). Therefore, the refinement of Cora to the SJs at the end of the larval period from its earlier localization spread along the lateral membrane depends on both Kune and Nrx.

The requirement for Cora to localize Nrx and Kune at 92 h AED is unexpected, as Cora was not required for barrier activity 92 h AED (Fig. 4A). This suggests there may be residual Kune activity in 92 h AED *Ap>*$cora^{RNAi}$ discs. We examined our localization data to determine whether we could detect residual Kune by comparing Kune signal at the apical-lateral junction and along the medial-lateral membrane in $cora^{RNAi}$- and $kune^{RNAi}$-expressing discs. At 92 h AED, we observed significantly higher Kune signal in both the apical and medial-lateral membranes of discs expressing $cora^{RNAi}$ compared with $kune^{RNAi}$ (Fig. S12A,B). In contrast, at 116 h AED we saw no additional Kune in the lateral membrane in discs expressing $cora^{RNAi}$ compared with $kune^{RNAi}$ (Fig. S12B,C). This suggests that at 92 h AED there may be a small fraction of Kune in the lateral membrane, the localization of which is not dependent on Cora. It is possible that this Cora-independent fraction of Kune may contribute to early barrier activity in the absence of Cora.

In summary, we see a complex interdependence between Kune, Nrx and Cora that determines their localization as the wing disc EB becomes increasingly impermeable during the third larval instar. These data indicate that, as the EB becomes more mature and impermeable, barrier activity becomes dependent on Cora as Cora localizes to the SJs.

Ecdysone signaling promotes epithelial barrier impermeability and Cora re-localization

The steroid hormone ecdysone is a crucial endocrine regulator of *Drosophila* development. During the third larval instar, pulses of ecdysone synthesis progressively increase the ecdysone titer throughout the larva, promoting imaginal disc growth and differentiation (Burdette, 1962; Colombani et al., 2005; Lavrynenko et al., 2015). Following imaginal disc damage and regeneration checkpoint activation, Dilp8 suppresses ecdysone synthesis through Lgr3 receptors in both the larval brain and PG (Hackney et al., 2012; Halme et al., 2010; Jaszczak et al., 2016).

To determine whether the changes in wing disc EB permeability are driven by ecdysone signaling, we first tested whether increasing the ecdysone titer in larvae would reduce disc barrier permeability. To do this, we transferred 80 h AED larvae to food containing either ethanol (control) or 0.6 mg/ml 20-hydroxyecdysone dissolved in ethanol. We assessed wing disc barrier function using our dextran infiltration assay at 98 h AED, when we previously observed the barrier to be more permeable to the dextran (Fig. 2C). This concentration of 20-hydroxyecdysone can alter the ecdysone titer without substantially accelerating pupariation time (Colombani et al., 2005; Jaszczak et al., 2015). In ecdysone-fed larvae, we saw that wing disc barrier permeability was substantially reduced when compared with wing discs from control larvae (Fig. 6A; Fig. S13), similar to that observed in more mature, 116 h AED wing discs (compare with Fig. 2C). This result indicates that increasing ecdysone promotes the development of the impermeable barrier we see as the third larval instar progresses.

To determine whether ecdysone acts directly on the wing disc and is necessary for the change in barrier permeability, we limited ecdysone signaling in the wing pouch by expressing a dominant-negative ecdysone receptor allele $EcR.A^{W650A}$ using *Bx-Gal4* and then assessed barrier function in wing discs. In 92 h AED discs, $EcR.A^{W650A}$ expression produced little effect on barrier permeability (Fig. 6B), demonstrating that the barrier function does not rely on ecdysone signaling at this earlier stage. However, in 116 h AED discs we saw that blocking ecdysone signaling produced a substantial increase in EB permeability (Fig. 6C). The expression of $EcR.A^{W650A}$ at 116 h AED did not produce the same disruption in barrier function as expression of $kune^{RNAi}$, rather it produced barrier permeability more similar to 92 h AED discs (compare Fig. 6B and C). These results demonstrate that ecdysone signaling in the wing disc is not necessary for barrier activity in 92 h AED wing discs, but is required for the development of the more impermeable barrier during the third instar.

As ecdysone-dependent barrier maturation in the wing discs during the third instar is associated with the re-localization of Cora away

Development (2021) 148, dev195057. doi:10.1242/dev.195057

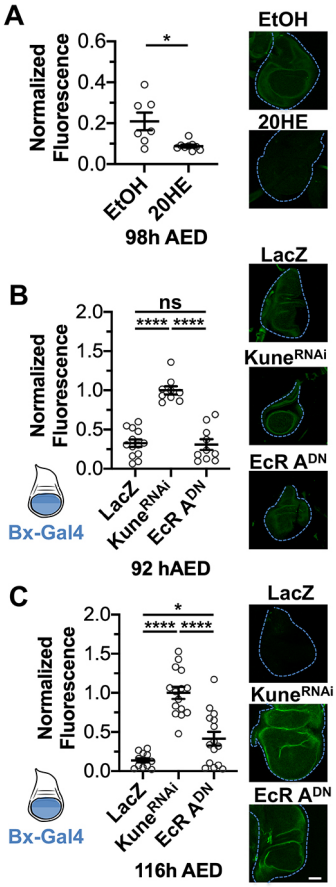

Fig. 6. Ecdysone induces barrier maturation. (A) Function of the wing disc EB at 98 h AED of larvae switched to food containing ethanol control (EtOH) or 0.6 mg/ml 20-hydroxecdysone (20HE) at 80 h AED. Normalized to *Ap>kune*^{RNAi}-expressing discs under the same feeding conditions (Fig. S9B). Representative images of fluorescein-conjugated 10 kD dextran localization for each condition are on the right. (B,C) EB function of *Bx>lacZ* (wild-type control), *Bx>kune*^{RNAi} and *Bx>EcR.A*^{DN} at 92 h (B) and 116 h AED (C). Barrier function is normalized to *Bx>kune*^{RNAi}-expressing discs under the same feeding conditions. Blue indicates expression area. Representative images of 10 kD dextran localization for each condition are on the right. Dashed blue lines indicate tissue outline defined by Actin (Rhodamine Phalloidin). Data are mean±s.e.m.; individual points represent single images. Left to right, n=7, 9 (A); n=13, 8, 10 (B); n=12, 15, 15 (C). ns, not significant. *P<0.05, ****P<0.0001 calculated by unpaired t-test with Welch's correction (A), ordinary one-way ANOVA with Tukey's multiple comparisons test (B) or Brown-Forsythe and Welch ANOVA tests with Dunnett's T3 multiple comparisons test (C). Scale bar: 50 µm.

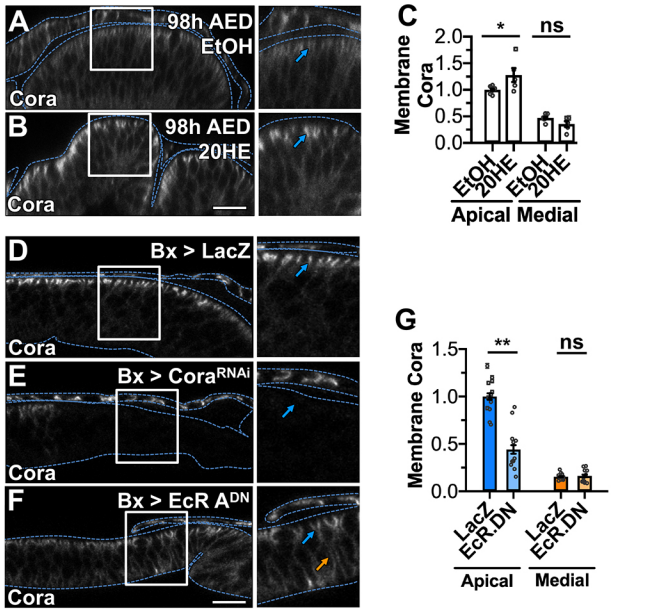

Fig. 7. Ecdysone induces Cora localization. (A-C) Localization of Cora in the wing imaginal discs of 98 h AED larvae switched to food containing ethanol control (EtOH) (A) or 0.6 mg/ml 20-hydroxecdysone (20HE; B) at 80 h AED. Dashed blue lines indicate tissue outline defined by Actin (Rhodamine Phalloidin; Fig. S14A,B). White box indicates magnified region shown in right panel. Blue arrows indicate apical-lateral localization. C shows quantification of Cora localized along the apical-lateral and medial-lateral membrane normalized to mean Cora membrane intensity from EtOH-fed control. (D-G) Localization of Cora in the wing imaginal discs in *Bx>lacZ* (wild-type control; D), *Bx>cora*^{RNAi} (E) and *Bx>EcR.A*^{DN} (F) at 116 h AED. Dashed lines indicate tissue outline defined by Actin (Rhodamine Phalloidin; Fig. S10). Tissues are oriented with the dorsal region on the right (*bx* expression dorsally is higher than ventrally). White box indicates magnified region shown in right panels. Blue arrows indicate apical-lateral Cora localization (or lack thereof). Orange arrow indicates medial-lateral localization of Cora that is observed in some regions of the tissue; this medial-lateral localization is not significant across the tissue. G shows quantification of Cora localized along the apical-lateral and medial-lateral membrane from *lacZ*- and *EcR.A*^{DN}-expressing wing discs at 116 h AED. Normalized to mean Cora membrane intensity from *Bx>lacZ*. (C,G) Individual points represent mean±s.e.m. for each image, with n as the number of cell-cell interactions. Bars represent mean±s.e.m. across the images, with n as the number of images. Details about the quantification method are explained in the Materials and Methods and Fig. S8. n=7 (A,C), 5 (B,C), 15 (D,G), 7 (E), 15 (F,G) images. ns, not significant. *P<0.05, **P<0.01 by one-way ANOVA with Tukey's multiple comparisons test (C) or Brown-Forsythe and Welch ANOVA with Dunnett's T3 multiple comparisons test (G). Scale bars: 10 µm.

from the lateral membrane specifically to the SJs, we wanted to determine whether this change in Cora localization also depends on ecdysone signaling. We first determined whether ecdysone signaling is sufficient to shift Cora localization to the apical-lateral membrane. To do this, we examined Cora localization in discs from 98 h AED larvae fed either ecdysone or control food. We saw that ecdysone feeding produced a small, but significant, increase in the apical-lateral localization of Cora (Fig. 7A-C; Fig. S14A-D,I). We also observed a small increase in Nrx localization at the apical-lateral junction (Fig. S14E,F,J), but no change in Kune localization (Fig. S14G,H,K). These data demonstrate that ecdysone feeding promotes the localization of Cora to the apical-lateral membrane, which could explain the greater EB impermeability we see in these discs.

To determine whether ecdysone signaling within the wing epithelium is necessary to promote the apical-lateral localization of Cora, we examined the cellular localization of Cora in 116 h AED control wing discs and wing discs expressing *EcR.A*^{W650A}. Inhibition of ecdysone signaling by *EcR.A*^{W650A} reduced Cora localization at the apical-lateral membrane, the site of SJs (Fig. 7D-G; Fig. S15). In some regions of the tissue, we also observed a redistribution of Cora along the lateral membrane similar to that observed earlier in 92 h AED discs (orange arrows, Fig. 7F); however, this redistribution pattern was not uniformly observed (Fig. 7G). The re-localization of Cora was consistent with the effect of *EcR.A*^{W650A} on the permeability of these discs, producing an increase in permeability similar to that seen in 92 h AED wing discs, but not completely disrupting the EB (Fig. 7C).

In summary, we see that at 92 h AED the EB activity of the wing disc is not dependent on ecdysone signaling. As the discs progress through development, Cora re-localizes specifically to the site of the SJ. Along with the increased impermeability of the EB, both are

Development (2021) 148, dev195057. doi:10.1242/dev.195057

dependent on ecdysone signaling within the wing imaginal disc epithelium.

The epithelial barrier regulates the duration of regenerative checkpoint delay

Our data indicate that ecdysone regulates maturation of the EB and that the EB limits Dilp8 signaling, leading us to question whether the EB determines the duration of the regenerative checkpoint. To test this, we targeted damage to the wing discs by using *Bx-Gal4* to express the TNFα homolog Eiger in the wing disc pouch (Igaki et al., 2002; Kauppila et al., 2003; Moreno et al., 2002) and examined the effects of barrier disruption on checkpoint duration. As we previously observed, *kune*^{RNAi} expression alone produced only a minor effect on delay, whereas Eiger expression in the wing disc produced a substantial delay of 57 h. When we co-expressed Eiger and *kune*^{RNAi}, we saw a synergistic effect on delay that was significantly longer than the expected additive effect of *kune*^{RNAi} and Eiger expression alone (80 h actual, 62 h additive; Fig. 8A; Fig. S16A). This additional delay was not associated with increased endogenous Dilp8 expression at 104 h AED (Fig. S17). We observed a similar result when the EB was disrupted with *nrx*^{RNAi} (Fig. S16B,C and S17). These data indicate that the EB limits regeneration checkpoint delay following damage.

As barrier disruption during regeneration extended regeneration checkpoint delay, we wanted to test whether this additional delay is accompanied by continued regenerative activity in the disc. To do this, we examined the expression of Dilp8 and Wingless during checkpoint delay. The strong expression of Dilp8 and Wingless in damaged tissues indicates regenerative activity in the wing disc. At the end of larval development, the expression of these two genes is suppressed, preventing regeneration and checkpoint activation in late larval discs (Harris et al., 2016). Using a GFP reporter for *dilp8* transcription and antibodies targeting Wingless (4D4; Developmental Studies Hybridoma Bank), we first examined *dilp8* and Wingless staining in undamaged tissues and observed little difference in the expression of both genes following barrier disruption by *kune*^{RNAi} (Fig. S18A-C). When we measured *dilp8* and Wingless expression in *Bx>eiger* or *Bx>kune*^{RNAi}*; eiger* tissues, we saw little difference in expression level of *dilp8* and Wingless throughout much of the checkpoint delay period (Fig. 8B-E; Fig. S18D-F). The only exception was that we saw slightly less *dilp8* expression in *Bx>kune*^{RNAi}*; eiger* discs at 116 h AED (Fig. S18E, 116 h AED). However, when we measured *dilp8* and Wingless expression in the extended delay period of *Bx>kune*^{RNAi}*; eiger* larvae, we saw that the expression of these regenerative markers not only persisted during the extended delay, but both were substantially upregulated during this period (Fig. 8C,E; Fig. S18E,F). In addition, we saw substantial overgrowth of the regenerating wing disc (Fig. S18D; compare 188 h AED with earlier timepoints or with Fig. S18A). It was unclear from our analysis whether the increased *dilp8* and Wingless expression and tissue overgrowth that we observed resulted from dysregulated regenerative activity in the disc or the extended growth period.

Together, these results demonstrate that disruption of the EB in damaged imaginal discs produces an extended larval period that can support persistent regenerative gene expression. This demonstrates that a fully-functional EB can limit the duration of damage-induced checkpoint delay, likely through the sequestration of Dilp8 within the imaginal disc lumen.

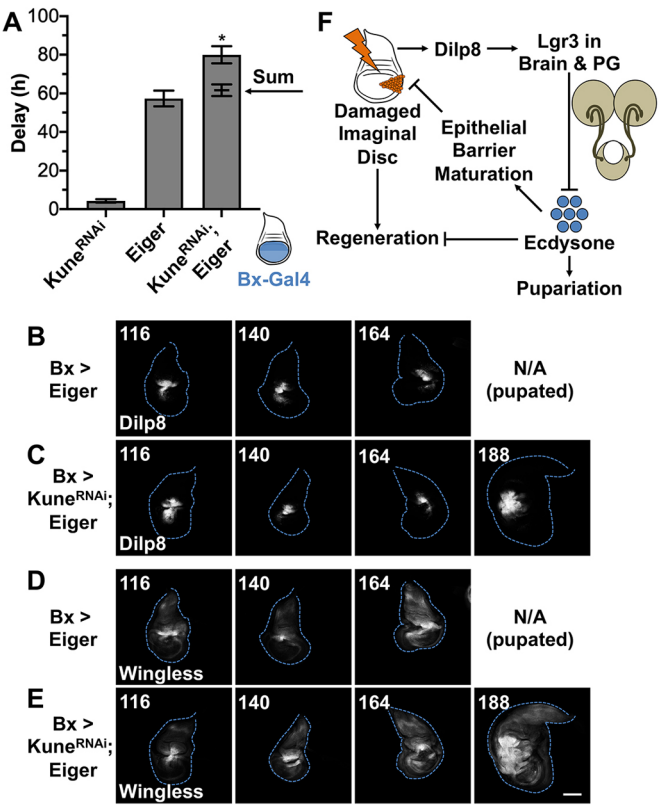

Fig. 8. The epithelial barrier regulates the duration of the regeneration checkpoint. (A) Expression of *kune*^{RNAi} in Eiger-damaged tissues induces synergistic delay. Data were collected from at least three independent experiments, bars represent mean±s.e.m. *P<0.05 from one sample t-test comparing the additive value and observed delay. (B-E) Timecourse from 116 h AED to pupation of Dilp8 (Dilp8^{MI00727} / +; B,C) and Wingless (anti-Wingless; D,E) localization and expression in wing imaginal discs following damage (*Bx>eiger*; top row) compared with damage and Kune knockdown (*Bx>kune*^{RNAi}*; eiger*; bottom row). Dashed blue lines indicate tissue boundaries defined by Actin (Rhodamine Phalloidin; Fig. S18D). Quantification of fluorescence in Fig. S18E,F. Undamaged control comparisons in Fig. S18A-C. Images are representative. Left to right: n=11, 15, 12 (B); 16, 15, 11, 7 (C); 7, 15, 12 (D); 14, 15, 10, and 9 (E) images. (F) Following damage to the imaginal discs, regeneration is initiated causing Dilp8 production and secretion from the damaged tissues. Dilp8 functions on Lgr3 receptors in the brain and PG to inhibit ecdysone production, resulting in a delay to pupariation. In the late third instar, high levels of ecdysone inhibit regenerative ability and also induce the maturation of the EB in imaginal discs. The EB inhibits Dilp8 signaling and regulates the duration of the regeneration checkpoint in development. Scale bar: 50 µm.

DISCUSSION

How is the end of the regeneration period determined?

The mechanisms for determining when the target of regeneration is reached remain poorly understood (Fox et al., 2020). Here, we demonstrate that the formation of a mature, impermeable EB determines the duration of the regenerative period by regulating Dilp8 signaling. As the EB of the wing disc causes Dilp8 accumulation in the imaginal disc lumen (Colombani et al., 2012; Fig. 1), we propose that the EB limits Dilp8 signaling by physically sequestering Dilp8 from the hemolymph, thereby preventing signaling in the brain and PG, in which Dilp8 acts through Lgr3 to inhibit ecdysone production (Colombani et al., 2012, 2015; Garelli et al., 2012, 2015; Jaszczak et al., 2016).

We propose that, as regeneration is completed, the balance between Dilp8 signaling and ecdysone signaling shifts to favor ecdysone signaling by the establishment of the mature, prepupal EB trapping Dilp8 in the regenerated disc lumen. Thus, the re-establishment of an impermeable EB would be one mechanism for epithelial tissues to communicate functional restoration and the completion of regeneration (Fig. 8F).

Development (2021) 148, dev195057. doi:10.1242/dev.195057

Regulated maturation of the epithelial barrier

We also demonstrate that barrier function changes during the third instar, growing more impermeable in response to ecdysone. Although we have not determined the direct target of ecdysone that produces this change, we observed that ecdysone refines Cora localization from being spread along the length of the lateral membrane to a specific localization at the SJs in the apical-lateral membrane. This re-localization correlates with the establishment of a mature, impermeable EB. This mechanism is similar to observations that Cora re-localizes to the SJs during embryonic stages 12 and 17 in the developing salivary gland and embryonic epidermis, during the establishment of the EB in these tissues (Hall and Ward, 2016; Oshima and Fehon, 2011; Paul et al., 2003). Similar to the third instar, ecdysone production peaks during this embryonic period and EcR is expressed in the embryonic salivary glands and epidermis (Kozlova and Thummel, 2000, 2003; Tan et al., 2014). We suggest that the regulation of Cora localization by ecdysone may be a general mechanism for the maturation of an impermeable barrier in developing *Drosophila* epithelia.

Our examination of EB maturation in the wing disc also raises questions about the role of Cora and Kune in barrier function at 92 h AED. The barrier at this time is more permeable than is observed later, but still limits the passage of 10 kD dextran (Fig. 2B). Kune, but not Cora, is required for this early barrier activity (Fig. 4); yet, when we blocked Cora expression with $cora^{RNAi}$, we saw that Cora was necessary for the localization of both Nrx and Kune at both 92 h and 116 h AED (Fig. 5). This suggests that in 92 h AED discs lacking Cora, Kune still retains some residual barrier activity, which is lost at 116 h AED. One possible explanation is that a low level of Kune may remain in Cora mutant tissues at 92 h AED but not at 116 h AED, and we observed some of this (Fig. S12). However, we cannot exclude that these observations might be due to differences in the dynamics of Cora and Kune knockdown. Closer examination will be necessary to better understand how each of these core components contributes to the barrier as the wing disc matures.

Could other signaling pathways be regulated by epithelial barrier maturation?

Our observation that Dilp8 is constrained by the wing disc EB raises the question of whether other signals are regulated by sequestration in the imaginal disc lumen. One possibility is the morphogen Decapentaplegic (Dpp, *Drosophila* BMP2/4 ortholog). Dpp has numerous roles in developmental growth and patterning in imaginal discs (Hamaratoglu et al., 2014). During larval development, Dpp produced in imaginal tissues inhibits ecdysone production in the PG early in the third larval instar (Setiawan et al., 2018). By the late third instar, Dpp is not detected in the larval hemolymph and Dpp activity in the PG ceases despite high levels of expression in imaginal discs (Setiawan et al., 2018). Setiawan et al. hypothesized that this could result from the trapping of Dpp in imaginal disc tissues and the dilution of circulating Dpp by increased hemolymph volume, but were unable to identify how the tissues trapped Dpp (Setiawan et al., 2018). Our data suggest that Dpp might be trapped in late third instar discs by the mature EB. Further experiments will be necessary to test this hypothesis.

In summary, our data demonstrate that in *Drosophila* ecdysone signaling alters the permeability of the wing disc EB during the final larval instar. We also show that a mature, impermeable wing disc EB limits Dilp8 signaling, determining the duration of the regenerative checkpoint. This provides a novel mechanism by which the barrier, a primary characteristic of epithelial tissues, can communicate the completion of regeneration.

MATERIALS AND METHODS

Drosophila stocks and husbandry

The fly stocks used were, or were generated from crosses with, Ap-Gal4; UAS-LacZ.NZ, UAS-Dcr2/SM6-TM6B [derived from Bloomington *Drosophila* Stock Center (BDSC), 3041], Bx-Gal4, UAS-Dcr2 (Dr David Bilder, University of California, Berkeley, CA, USA), UAS-LacZ.NZ (BDSC, 3956), UAS-Kune[RNAi] [Vienna *Drosophila* Resource Center (VDRC), GD3962], UAS-NrxIV[RNAi] (VDRC, GD8353), UAS-Sinu[RNAi] (VDRC, GD44928), UAS-Cora[RNAi] (BDSC, 51845), UAS-EcR.A.W650A (BDSC, 9451), NrxIV-GFP (BDSC, 50798), UAS-eiger, UAS-Dilp8::3xFLAG (Dr Maria Dominguez, Universidad Miguel Hernández, Spain) (Garelli et al., 2012), and Dilp8::GFP (BDSC, 33079).

Stocks and crosses were maintained in 25°C incubators with a 12-h alternating light-dark cycle. Developmental timing was synchronized through egg staging, with collection from a 4-h egg-laying interval on grape agar plates (Genesee Scientific) with a small amount of baker's yeast paste. At 24 h AED, 20-30 first instar larvae were transferred into vials containing cornmeal-yeast-molasses media (Archon Scientific, B101). Ecdysone food was prepared by dissolving 1.2 mg 20-hydroxyecdysone (Sigma-Aldrich) dissolved in 95% ethanol in 2 ml of food media (final concentration 0.6 mg/ml), or an equivalent volume of ethanol for control. Larvae were reared as previously described (Halme et al., 2010) until 80 h AED then transferred to the ecdysone or ethanol-control food, approximately six larvae per vial. For specific genotypes used in each figure see Supplementary Materials and Methods.

Pupariation time and developmental delay

Larvae were raised as described above. For calculating purposes, 0 h AED was considered to be the middle of the egg laying interval. The number of pupae in each vial was counted approximately every 12 h starting ∼104 h AED and ending 2 days after the most recent pupation. To simplify calculations, data were pooled from multiple vials of the same genotype that were laid on the same day. Data from separate lays were calculated separately, at least three lays are represented in each experiment. An estimated median pupariation time was then calculated:

$$\text{Median} = T1 + \left((T2 - T1) \times \frac{0.5 - S1}{S2 - S1} \right). \quad (1)$$

Developmental delay was considered to be the difference in pupariation time between the experimental and control groups. Estimated median pupariation time was calculated by first determining the sum fraction of total pupae counted at each timepoint for each genotype. The first timepoint to have sum fraction of total pupae exceeding 50% indicates that the median pupariation time occurred between that timepoint and the proceeding timepoint. We next calculated how long past the proceeding timepoint 50% of larvae pupated as well as the difference between the sum fractions. To estimate how far past the first timepoint the median pupariation time was, we divided the difference from the halfway point by the difference between the sum fractions then multiplied this by the difference between the timepoints. We then added this number to the preceding timepoint. $T2$ indicates the later timepoint, $T1$ indicates the earlier timepoint, $S2$ indicates the sum fraction of pupae at $T2$, $S1$ indicates the sum fraction of pupae at $T1$.

Dissection and immunofluorescent staining

Larvae were inverted and cleaned in PBS then fixed with 4% paraformaldehyde in PBS (20 min) and washed with PBS (twice for 5 min each). The tissues were permeabilized with 0.3% Triton in PBS (twice for 10 min each) then washed with a blocking solution of 10% goat serum and 0.1% Triton in PBS (30 min). Then the tissues were incubated, rocking in primary antibody solutions (overnight at 4°C or for 2-4 h at room temperature). The process was repeated for secondary antibodies and then the tissues were incubated rocking in 80% glycerol in PBS (overnight at 4°C). The tissues were stored at 4°C in 80% glycerol and were mounted for imaging within 1 week of staining. Imaginal discs were isolated from the stained tissues and mounted on glass slides with Vectashield (Vector Laboratories). Cross-section images were taken from tissues mounted on slides with the coverslips raised by double-sided tape. For experiments with

Development (2021) 148, dev195057. doi:10.1242/dev.195057

Kune or FLAG staining, the above procedure was modified to reduce non-specific staining. In these experiments, larvae were dissected in Schneider's Insect Medium (Sigma-Aldrich), fixed in 4% paraformaldehyde in Schneider's Insect Medium, stained in 1 day, within 3 days of dissection, and imaged within 3 days of staining.

Antibody solutions were prepared in 10% goat serum and 0.1% Triton in PBS. The primary antibodies used were: mouse β-Gal (1:250; Promega, #Z378A), mouse anti-Cora C615.16 (1:400; Developmental Studies Hybridoma Bank, #C615.16), mouse anti-FLAG M2 F1804 (1:250; Sigma-Aldrich, #F1804), mouse 4D4 anti-Wingless (1:100; Developmental Studies Hybridoma Bank, #4D4), rabbit β-Gal (1:400; MP Biomedicals, #559761), rabbit anti-cleaved Dcp-1 (1:500, Cell Signaling Technology, #9578S), rabbit anti-phospho Histone H3 (1:100, Millipore, #06-570) and rabbit anti-Kune (1:1000; Dr Mikio Furuse; Nelson et al., 2010). The secondary antibodies used were: goat anti-mouse or anti-rabbit Alexa405, Alexa488 or Alexa633 (1:1000; Thermo Fisher Scientific, #A-31556, #A-11008, #A-21050, #A-21070). F-actin was identified by Rhodamine-conjugated Phalloidin (1:100; Thermo Fisher Scientific) staining that was performed concurrently with secondary antibody incubations.

Imaging and statistical analysis

Confocal imaging was carried out using an Olympus FluoView 1000 (Figs 2,4,6,7D-F; Figs S3B-D,S5,S13,S15) within the University of Virginia Department of Cell Biology and a Zeiss LSM 700 (Figs 1C-E,3,5,7A,B,8; Figs S1,S3A,S4,S7-S11,S14,S17,S18) in the University of Virginia Advanced Microscopy Facility (RRID:SCR_018736). Laser power and gain settings for each set of stained samples were based on the experimental group with the highest fluorescence intensity in each channel, and kept constant within the experiment. To compare between independently repeated experiments, we normalized within the experiment as indicated. Images were processed and quantified using Fiji/ImageJ (Schindelin et al., 2012). Prism 8 software was used for statistical analysis. The statistical tests used are listed in the figure descriptions.

Dextran assay

Larvae were inverted and cleaned in Schneider's Insect Medium, transferred into a 1:8 dilution of 10 kD fluorescein-conjugated dextran (Invitrogen) in Schneider's Insect Medium and incubated, rocking and covered, at room temperature for 30 min. The tissues were washed briefly (~1 min) in Schneider's Insect Medium to remove excess dextran, then fixed with 4% paraformaldehyde in Schneider's Insect Medium. Tissues were washed, stained, and imaged as described above.

Fluorescent dextran infiltration was measured using Fiji/ImageJ (Schindelin et al., 2012), taking the mean intensity along a line in the imaginal disc lumen (identified by Rhodamine Phalloidin or Cora staining) and subtracting background from outside the disc area. Discs that appeared punctured were either not measured or categorized separately from intact discs. The fluorescence intensity varies with each experiment, so the data were normalized to the mean from controls that were incubated simultaneously.

Quantification of septate junction component localization

SJ localization was quantified using Fiji/ImageJ (Schindelin et al., 2012). Two lines were drawn to collect fluorescence intensity of the junctions. The first across the apical surface of cells near the center of where the SJs were localized, and the second along the middle of the cells. Junctional intensity, or membrane intensity for the medial region, was considered as an average of the 7 pixels surrounding local maxima. In this way we hoped to average out misrepresentations in the data that arose from slices that cut through cells approximately parallel to the cell membranes and from slices that cut through tricellular junctions and had more protein from the third cell. None of the proteins we looked at are reported or appeared to have specific tricellular activity. We then took the ratio of the average junctional peak intensity to the average medial peak intensity (Fig. S7).

Peak identification was adjusted in three steps to reduce false identification of a membrane peak due to the noise within an image, especially with regards to anti-Kune and anti-Cora staining. First, to ensure the peak was not a result of a slightly brighter random pixel, we removed peaks that were below the median fluorescence of the entire line. Second, to ensure the identified peak was localized at the membrane, we removed points of anti-Kune and anti-Cora staining that did not have an Nrx-GFP peak within the same 7-pixel range. We used Nrx-GFP for this instead of Actin (Rhodamine Phalloidin) in all figures except Fig. 7G (this experiment was not carried out with an Nrx-GFP background), because Nrx-GFP has extremely low noise as it is a membrane-bound GFP produced within the cell and does not need to be stained for. Nrx-GFP also has a very high association with the membrane even away from canonical apical-lateral staining; although this fluorescence is very dim, it is still detectable and highly correlated with the membrane. Finally, to ensure that we took a measurement at the membrane and not at a noisy region within the cell, if no anti-Kune or anti-Cora peak was identified within the 7-pixel range of the Nrx-GFP peak, a measurement was added at the same placement of the Nrx-GFP peak. Together, these adjustments reduced the number of peak identifications in each image by approximately one to ten junctions depending on the stain (most images had 40-60 junctions following adjustments).

Quantification of Wingless and Dilp8

Wingless and Dilp8 fluorescence were quantified using Fiji/ImageJ (Schindelin et al., 2012). The region of quantification was determined differently in undamaged tissues than it was in tissues damaged by Eiger expression (described below). In these the quantification region sum fluorescence was measured. Fluorescence background was taken to be the minimum fluorescence in the measurement region. Data are normalized as indicated in the figure legends.

In undamaged wing imaginal discs, Wingless was quantified in the dorsal hinge of the imaginal disc pouch by tracing Wingless in this region from the dorsal edge of the margin. Marginal and ventral hinge Wingless were not quantified as undamaged 116 h AED wing discs are evaginating, which produces tissue folding in these regions. Dilp8 fluorescence was quantified in the pouch region of the discs as defined by the outer edge of hinge Wingless (not just the dorsal hinge). In damaged tissues, both Wingless and Dilp8 fluorescence were collected from the approximate area of the blastema to exclude background from notum expression.

Acknowledgements

The authors would like to acknowledge Dr David Bilder, Dr Pierre Leopold, Dr Maria Dominguez, Dr Mikio Furuse and Dr Robert Ward for reagents and/or *Drosophila* stocks crucial for the completion of these experiments. The authors would like to acknowledge the University of Virginia Advanced Microscopy Facility (RRID: SCR_018736) for training and access to the LSM700 confocal microscope.

Competing interests

The authors declare no competing or financial interests.

Author contributions

Conceptualization: D.D., R.Y., A.H.; Methodology: D.D., R.B., R.Y., A.H.; Validation: D.D.; Formal analysis: D.D., R.B., F.K., A.H.; Investigation: D.D., R.B., F.K.; Resources: A.H.; Writing - original draft: D.D., A.H.; Writing - review & editing: D.D., A.H.; Supervision: A.H.; Project administration: A.H.; Funding acquisition: A.H.

Funding

This work was supported by the National Institutes of Health (GM099803 to A.H., GM008136 to D.D., and GM008715 to F.K.) and the March of Dimes Foundation (5FY1260 to A.H.). Deposited in PMC for release after 12 months.

Supplementary information

Supplementary information available online at
https://dev.biologists.org/lookup/doi/10.1242/dev.195057.supplemental

Peer review history

The peer review history is available online at
https://dev.biologists.org/lookup/doi/10.1242/dev.195057.reviewer-comments.pdf

References

Baumgartner, S., Littleton, J. T., Broadie, K., Bhat, M. A., Harbecke, R., Lengyel, J. A., Chiquet-Ehrismann, R., Prokop, A. and Bellen, H. J. (1996). A Drosophila neurexin is required for septate junction and blood-nerve barrier formation and function. *Cell* **87**, 1059-1068. doi:10.1016/S0092-8674(00)81800-0

Burdette, W. J. (1962). Changes in titer of ecdysone in Bombyx mori during metamorphosis. *Science* **135**, 432-432. doi:10.1126/science.135.3502.432

Buszczak, M., Paterno, S., Lighthouse, D., Bachman, J., Planck, J., Owen, S., Skora, A. D., Nystul, T. G., Ohlstein, B., Allen, A. et al. (2007). The carnegie protein trap library: a versatile tool for drosophila developmental studies. *Genetics* **175**, 1505-1531. doi:10.1534/genetics.106.065961

Cohen, B., McGuffin, M. E., Pfeifle, C., Segal, D. and Cohen, S. M. (1992). apterous, a gene required for imaginal disc development in Drosophila encodes a member of the LIM family of developmental regulatory proteins. *Genes Dev.* **6**, 715-729. doi:10.1101/gad.6.5.715

Colombani, J., Bianchini, L., Layalle, S., Pondeville, E., Dauphin-Villemant, C., Antoniewski, C., Carré, C., Noselli, S. and Léopold, P. (2005). Antagonistic actions of ecdysone and insulins determine final size in Drosophila. *Science* **310**, 667-670. doi:10.1126/science.1119432

Colombani, J., Andersen, D. S. and Léopold, P. (2012). Secreted peptide Dilp8 coordinates Drosophila tissue growth with developmental timing. *Science* **336**, 582-585. doi:10.1126/science.1216689

Colombani, J., Andersen, D. S., Boulan, L., Boone, E., Romero, N., Virolle, V., Texada, M. and Léopold, P. (2015). Drosophila Lgr3 couples organ growth with maturation and ensures developmental stability. *Curr. Biol.* **25**, 2723-2729. doi:10.1016/j.cub.2015.09.020

Fehon, R. G., Dawson, I. A. and Artavanis-Tsakonas, S. (1994). A Drosophila homologue of membrane-skeleton protein 4.1 is associated with septate junctions and is encoded by the coracle gene. *Development* **120**, 545-557.

Fox, D. T., Cohen, E. and Smith-Bolton, R. (2020). Model systems for regeneration: Drosophila. *Development* **147**, dev173781. doi:10.1242/dev.173781

Furuse, M. and Tsukita, S. (2006). Claudins in occluding junctions of humans and flies. *Trends Cell Biol.* **16**, 181-188. doi:10.1016/j.tcb.2006.02.006

Garelli, A., Gontijo, A. M., Miguela, V., Caparros, E. and Dominguez, M. (2012). Imaginal discs secrete insulin-like peptide 8 to mediate plasticity of growth and maturation. *Science* **336**, 579-582. doi:10.1126/science.1216735

Garelli, A., Heredia, F., Casimiro, A. P., Macedo, A., Nunes, C., Garcez, M., Dias, A. R. M., Volonte, Y. A., Uhlmann, T., Caparros, E. et al. (2015). Dilp8 requires the neuronal relaxin receptor Lgr3 to couple growth to developmental timing. *Nat. Commun.* **6**, 8732. doi:10.1038/ncomms9732

Genova, J. L. and Fehon, R. G. (2003). Neuroglian, Gliotactin, and the Na+/k+ ATPase are essential for septate junction function in Drosophila. *J. Cell Biol.* **161**, 979-989. doi:10.1083/jcb.200212054

Hackney, J. F. and Cherbas, P. (2014). Injury response checkpoint and developmental timing in insects. *Fly* **8**, 226-231. doi:10.1080/19336934.2015.1034913

Hackney, J. F., Zolali-Meybodi, O. and Cherbas, P. (2012). Tissue damage disrupts developmental progression and ecdysteroid biosynthesis in Drosophila. *PloS one* **7**, e49105. doi:10.1371/journal.pone.0049105

Hall, S. and Ward, R. E. (2016). Septate junction proteins play essential roles in morphogenesis throughout embryonic development in Drosophila. *G3 (Bethesda, Md.)* **6**, 2375-2384. doi:10.1534/g3.116.031427

Halme, A., Cheng, M. and Hariharan, I. K. (2010). Retinoids regulate a developmental checkpoint for tissue regeneration in Drosophila. *Curr. Biol.* **20**, 458-463. doi:10.1016/j.cub.2010.01.038

Hamaratoglu, F., Affolter, M. and Pyrowolakis, G. (2014). Dpp/BMP signaling in flies: from molecules to biology. *Semin. Cell Dev. Biol.* **32**, 128-136. doi:10.1016/j.semcdb.2014.04.036

Harris, R. E., Setiawan, L., Saul, J. and Hariharan, I. K. (2016). Localized epigenetic silencing of a damage-activated WNT enhancer limits regeneration in mature Drosophila imaginal discs. *eLife* **5**, e11588. doi:10.7554/eLife.11588

Igaki, T., Kanda, H., Yamamoto-Goto, Y., Kanuka, H., Kuranaga, E., Aigaki, T. and Miura, M. (2002). Eiger, a TNF superfamily ligand that triggers the Drosophila JNK pathway. *EMBO J.* **21**, 3009-3018. doi:10.1093/emboj/cdf306

Izumi, Y. and Furuse, M. (2014). Molecular organization and function of invertebrate occluding junctions. *Semin. Cell Dev. Biol.* **36**, 186-193. doi:10.1016/j.semcdb.2014.09.009

Jaszczak, J. S., Wolpe, J. B., Dao, A. Q. and Halme, A. (2015). Nitric oxide synthase regulates growth coordination during Drosophila melanogaster imaginal disc regeneration. *Genetics* **200**, 1219-1228. doi:10.1534/genetics.115.178053

Jaszczak, J. S., Wolpe, J. B., Bhandari, R., Jaszczak, R. G. and Halme, A. (2016). Growth Coordination during Drosophila melanogaster Imaginal disc regeneration is mediated by signaling through the relaxin receptor Lgr3 in the prothoracic gland. *Genetics* **204**, 703-709. doi:10.1534/genetics.116.193706

Kauppila, S., Maaty, W. S. A., Chen, P., Tomar, R. S., Eby, M. T., Chapo, J., Chew, S., Rathore, N., Zachariah, S., Sinha, S. K. et al. (2003). Eiger and its receptor, Wengen, comprise a TNF-like system in Drosophila. *Oncogene* **22**, 4860-4867. doi:10.1038/sj.onc.1206715

Khadilkar, R. J. and Tanentzapf, G. (2019). Septate junction components control Drosophila hematopoiesis through the Hippo pathway. *Development* **146**, dev166819. doi:10.1242/dev.166819

Kozlova, T. and Thummel, C. S. (2000). Steroid regulation of postembryonic development and reproduction in Drosophila. *Trends Endocrinol. Metab.* **11**, 276-280. doi:10.1016/S1043-2760(00)00282-4

Kozlova, T. and Thummel, C. S. (2003). Essential roles for ecdysone signaling during Drosophila mid-embryonic development. *Science* **301**, 1911-1914. doi:10.1126/science.1087419

Lamb, R. S., Ward, R. E., Schweizer, L. and Fehon, R. G. (1998). Drosophila coracle, a member of the protein 4.1 superfamily, has essential structural functions in the septate junctions and developmental functions in embryonic and adult epithelial cells. *Mol. Biol. Cell* **9**, 3505-3519. doi:10.1091/mbc.9.12.3505

Lavrynenko, O., Rodenfels, J., Carvalho, M., Dye, N. A., Lafont, R., Eaton, S. and Shevchenko, A. (2015). The ecdysteroidome of Drosophila: influence of diet and development. *Development* **142**, 3758-3768. doi:10.1242/dev.124982

Lee, S.-R., Hong, S.-T. and Choi, K.-W. (2020). Regulation of epithelial integrity and organ growth by Tctp and Coracle in Drosophila. *PLoS Genet.* **16**, e1008885. doi:10.1371/journal.pgen.1008885

Milán, M., Diaz-Benjumea, F. J. and Cohen, S. M. (1998). Beadex encodes an LMO protein that regulates Apterous LIM-homeodomain activity in Drosophila wing development: a model for LMO oncogene function. *Genes Dev.* **12**, 2912-2920. doi:10.1101/gad.12.18.2912

Moreno, E., Yan, M. and Basler, K. (2002). Evolution of TNF signaling mechanisms: JNK-dependent apoptosis triggered by Eiger, the Drosophila homolog of the TNF superfamily. *Curr. Biol.* **12**, 1263-1268. doi:10.1016/S0960-9822(02)00954-5

Morin, X., Daneman, R., Zavortink, M. and Chia, W. (2001). A protein trap strategy to detect GFP-tagged proteins expressed from their endogenous loci in Drosophila. *Proc. Natl. Acad. Sci. USA* **98**, 15050-15055. doi:10.1073/pnas.261408198

Nelson, K. S., Furuse, M. and Beitel, G. J. (2010). The Drosophila Claudin Kune-kune is required for septate junction organization and tracheal tube size control. *Genetics* **185**, 831-839. doi:10.1534/genetics.110.114959

Oshima, K. and Fehon, R. G. (2011). Analysis of protein dynamics within the septate junction reveals a highly stable core protein complex that does not include the basolateral polarity protein Discs large. *J. Cell Sci.* **124**, 2861-2871. doi:10.1242/jcs.087700

Pastor-Pareja, J. C., Grawe, F., Martín-Blanco, E. and García-Bellido, A. (2004). Invasive cell behavior during Drosophila imaginal disc eversion is mediated by the JNK signaling cascade. *Dev. Cell* **7**, 387-399. doi:10.1016/j.devcel.2004.07.022

Paul, S. M., Ternet, M., Salvaterra, P. M. and Beitel, G. J. (2003). The Na^+/K^+ ATPase is required for septate junction function and epithelial tube-size control in the Drosophila tracheal system. *Development* **130**, 4963-4974. doi:10.1242/dev.00691

Schindelin, J., Arganda-Carreras, I., Frise, E., Kaynig, V., Longair, M., Pietzsch, T., Preibisch, S., Rueden, C., Saalfeld, S., Schmid, B. et al. (2012). Fiji: an open-source platform for biological-image analysis. *Nat. Methods* **9**, 676-682. doi:10.1038/nmeth.2019

Setiawan, L., Pan, X., Woods, A. L., O'Connor, M. B. and Hariharan, I. K. (2018). The BMP2/4 ortholog Dpp can function as an inter-organ signal that regulates developmental timing. *Life Sci. Alliance* **1**, e201800216. doi:10.26508/lsa.201800216

Suzuki, H., Tani, K., Tamura, A., Tsukita, S. and Fujiyoshi, Y. (2015). Model for the architecture of claudin-based paracellular ion channels through tight junctions. *J. Mol. Biol.* **427**, 291-297. doi:10.1016/j.jmb.2014.10.020

Tan, K. L., Vlisidou, I. and Wood, W. (2014). Ecdysone mediates the development of immunity in the Drosophila embryo. *Curr. Biol.* **24**, 1145-1152. doi:10.1016/j.cub.2014.03.062

Tepass, U., Tanentzapf, G., Ward, R. and Fehon, R. (2001). Epithelial cell polarity and cell junctions in Drosophila. *Annu. Rev. Genet.* **35**, 747-784. doi:10.1146/annurev.genet.35.102401.091415

Vallejo, D. M., Juarez-Carreño, S., Bolivar, J., Morante, J. and Dominguez, M. (2015). A brain circuit that synchronizes growth and maturation revealed through Dilp8 binding to Lgr3. *Science (New York, N.Y.)* **350**, aac6767. doi:10.1126/science.aac6767

Ward IV, R. E., Schweizer, L., Lamb, R. S. and Fehon, R. G. (2001). The protein 4.1, ezrin, radixin, moesin (FERM) domain of drosophila coracle, a cytoplasmic component of the septate junction, provides functions essential for embryonic development and imaginal cell proliferation. *Genetics* **159**, 219-228.